Supporting Information

Chen et al. 10.1073/pnas.1421927112

SI Materials and Methods

Cloning, Expression, and Purification. The PCR products of full-length (873 bp) and C-terminal domain truncated (723 bp) *spo0J* from *Helicobacter pylori* 26695 genomic DNA (*Hpspo0J*) were ligated into the BamHI and SalI sites of pQE30 (Qiagen), including a 12-residue hexahistidine tag (MRGSHHHHHHGS), and were then individually transformed into *E. coli* SG13009. The expression systems were incubated overnight at 37 °C in Luria-Bertani broth containing ampicillin and kanamycin. Expression of full-length *Hp*Spo0J (residues 1–290) and Ct-*Hp*Spo0J (residues 1–240) were induced by addition of isopropyl thiogalactopyranoside (IPTG) (0.4 mM, final concentration), and the cultures were then incubated at 20 °C for 20 h. Each cell pellet was suspended in lysis buffer (20 mM Tris·HCl, pH 8.0, 420 mM NaCl, and 5 mM $MgCl_2$). The pellets were homogenized, and the lysate was centrifuged. *Hp*Spo0J and Ct-*Hp*Spo0J were purified by Ni-NTA affinity (GE Healthcare) and eluted with elution buffer (20 mM Tris·HCl, pH 8.0, 420 mM NaCl, 110 mM imidazole, and 5 mM $MgCl_2$). Purified *Hp*Spo0J and Ct-*Hp*Spo0J were dialyzed against with reaction buffer (20 mM Tris·HCl, pH 8.0, 210 mM NaCl, and 5 mM $MgCl_2$) for crystallization. Because no homologous Ct-*Hp*Spo0J structure has been solved, the selenomethionine-substituted Ct-*Hp*Spo0J crystal was prepared for structural phase determination by the multiwavelength anomalous dispersion method (1). SeMet-Ct-*Hp*Spo0J protein was expressed from *E. coli* T7 express competent cells (New England BioLabs) and purified by His-tagged affinity chromatography in a manner similar to that used for Ct-*Hp*Spo0J.

***parS* DNA.** Equal molar concentrations of the double-stranded 24-bp DNA fragment (5′-AGGGTGTTCCACGTGAAACAGGGA-3′ and its complement 5′-TCCCTGTTTCACGTGGAACACCCT-3′) were annealed at 99 °C for 5 min and cooled to room temperature to form double-strand *parS*, which was stored at 4 °C before use. The 16-bp *parS* complementary sequences are underlined (2).

SEC-MALS. SEC-MALS was performed using an FPLC (fast protein liquid chromatography) purification system with a high-performance size-exclusion column (GE Healthcare) coupled to a Wyatt Dawn Heleos II light-scattering detector (Wyatt Technology). The full-length *Hp*Spo0J (4 mg/mL), the *Hp*Spo0J-*parS* complex (4 mg/mL), and Ct-*Hp*Spo0J (5 mg/mL), each in elution buffer, were applied to the size exclusion column. The molecular weights were determined using the static light scattering data in combination with the refractive index measurements (Wyatt Optilab rEX, connected downstream of the LS detector; Fig. S1).

Fluorescence Anisotropy. Fluorescence anisotropy measurements were performed using a Hitachi Fluorescence Spectrometer F4000. The excitation and emission wavelengths, 495 and 521 nm, respectively, were applied. Two DNA fragments, *parS* and a random sequence (5′-AAAACAAACCCAAAACAAACCC-3′) (3), were used, and the fluorescein-labeled single and double-stranded DNAs were made. Ct-*Hp*Spo0J (0–20 μM) was titrated into 500 nM fluoresceinated DNA samples (*parS*-containing dsDNA, *parS*-containing ssDNA, random dsDNA, and random ssDNA) in the reaction buffer (Fig. 1*B*). The data were fitted using Prism (GraphPad Software) to determine the dissociation constant (K_d).

Multiple Sequence Alignment of ParB Superfamily. The sequence alignment of *Hp*Spo0J and ParB homologous from *T. thermophilus* (*Tt*Spo0J), *B. subtilis* (*Bs*Spo0J), *P. aeruginosa* (*Pa*ParB), *C. crescentus* (*Cc*P1ParB), and *Enterobacteria phage* P1 (P1 ParB) is shown (Fig. S4). From the multiple sequence alignment (ClustalW), *Hp*Spo0J shared a high identity/similarity (~39/58%) with them except P1 ParB (15/26%). These proteins have similar secondary structures (4).

Data Collection and Processing. X-ray diffraction data of the Ct-*Hp*Spo0J–*parS* complex crystal was collected to 3.1-Å resolution. The datasets were indexed, integrated, and scaled using HKL-2000 (5). The Ct-*Hp*Spo0J–*parS* crystal belongs to the primitive monoclinic space group $P2_1$ with a unit cell parameters of a = 54.5 Å, b = 232.7 Å, c = 78.3 Å, and β = 109.2°. The Matthews coefficient (V_M) (6) was calculated as 2.53 $Å^3$/Da, with a solvent content of 51%, containing four molecules per asymmetric unit. For the phase determination, anomalous data from the SeMet-Ct-*Hp*Spo0J–*parS* crystal were collected. Detailed data statistics are summarized in Table S3.

Structure Determination and Refinement. The structural phase of the Ct-*Hp*Spo0J–*parS* complex was determined by the SeMet-MAD method (1). The selenium sites were identified with SHARP (7). The preliminary structural model can be built by SHARP automatically, and the entire model was completed manually with the COOT software (8). The structural refinement was carried out using CNS (9) and PHENIX (10). PROCHECK (11) was used to evaluate the stereochemistry and to identify the secondary structural elements. The Ct-*Hp*Spo0J–*parS* complex contains four molecules (chains A, B, C, and D) and two *parS* per asymmetric unit. The residues were determined in chains A (#55–226), B (# 35–226), C (#45–227), and D (#51–226). The structural model was refined to an R-factor of 25.1% and an R_{free} of 29.9% at 3.1 Å. The refinement statistics are summarized in Table S3.

SAXS. SAXS data for the full-length *Hp*Spo0J (3 mg/mL) were collected at 20 °C. The X-ray wavelength was 0.88 Å (14.0 keV), and the collection time was 300 s. The solvent blank buffer was 20 mM Tris·HCl, pH 8.0, 420 mM NaCl, 110 mM imidazole, and 5 mM $MgCl_2$ for gel filtration. Data were collected for a total q ($q = 4\pi\sin\theta/\lambda$) from 0.0066 to 0.3236 $Å^{-1}$. Background scattering from the buffer was subtracted, and data were scaled using PRIMUS (12). Primary data reduction was performed using an in-house program, and the processed data were analyzed using the ATSAS package software (13) (Fig. S6*A*). The radius of gyration (Rg) was calculated to be 46.9 Å from a Guinier plot using PRIMUS (12) and GNOM (14). The pair distance distribution function $P(r)$ and the maximum intramolecular distance D_{max} (175 Å) were calculated using GNOM (14) (Fig. S6*B*). A low-resolution SAXS model of *Hp*Spo0J was determined in ab initio from the SAXS data by DAMMIN (15). Averaged surface envelope was modeled by DAMEVER (12). The structural model of full-length *Hp*Spo0J can be built by the C-terminal domain of P1 ParB (residues 275–333; PDB ID code 1ZX4) (16) and the structure of the Ct-*Hp*Spo0J–*parS* complex (this study). The SAXS data were fitted with this structural model using FoXS ($\chi \sim 4.27$) (17, 18) (Fig. S6*C*). The full-length *Hp*Spo0J structural model was situated into the averaged surface envelope of the SAXS model by SUPCOMB (19).

1. Hendrickson WA, Ogata CM (1997) Phase determination from multiwavelength anomalous diffraction measurements. *Methods Enzymol* 276(Macromolecular Crystallography, Part A):494–523.
2. Lin DC, Grossman AD (1998) Identification and characterization of a bacterial chromosome partitioning site. *Cell* 92(5):675–685.
3. Leonard TA, Butler PJ, Löwe J (2005) Bacterial chromosome segregation: Structure and DNA binding of the Soj dimer—A conserved biological switch. *EMBO J* 24(2): 270–282.
4. Schumacher MA (2008) Structural biology of plasmid partition: Uncovering the molecular mechanisms of DNA segregation. *Biochem J* 412(1):1–18.
5. Otwinowski Z, Minor W (1997) Processing of X-ray diffraction data collected in oscillation mode. *Methods Enzymol* 276(Macromolecular Crystallography, Part A): 307–326.
6. Matthews BW (1968) Solvent content of protein crystals. *J Mol Biol* 33(2):491–497.
7. Vonrhein C, Blanc E, Roversi P, Bricogne G (2007) Automated structure solution with autoSHARP. *Methods Mol Biol* 364:215–230.
8. Emsley P, Lohkamp B, Scott WG, Cowtan K (2010) Features and development of Coot. *Acta Crystallogr D Biol Crystallogr* 66(Pt 4):486–501.
9. Brünger AT, et al. (1998) Crystallography & NMR system: A new software suite for macromolecular structure determination. *Acta Crystallogr D Biol Crystallogr* 54(Pt 5): 905–921.
10. Adams PD, et al. (2002) PHENIX: building new software for automated crystallographic structure determination. *Acta Crystallogr D Biol Crystallogr* 58(Pt 11): 1948–1954.
11. Laskowski RA, Macarthur MW, Moss DS, Thornton JM (1993) Procheck: A program to check the stereochemical quality of protein structures. *J Appl Cryst* 26(2):283–291.
12. Konarev PV, Volkov VV, Sokolova AV, Koch MHJ, Svergun DI (2003) PRIMUS: A Windows PC-based system for small-angle scattering data analysis. *J Appl Cryst* 36(5): 1277–1282.
13. Petoukhov MV, Konarev PV, Kikhney AG, Svergun DI (2007) ATSAS 2.1: Towards automated and web-supported small-angle scattering data analysis. *J Appl Cryst* 40(Suppl 1):S223–S228.
14. Svergun DI (1992) Determination of the regularization parameter in indirect-transform methods using perceptual criteria. *J Appl Cryst* 25(4):495–503.
15. Svergun DI (1999) Restoring low resolution structure of biological macromolecules from solution scattering using simulated annealing. *Biophys J* 77(5):2896.
16. Schumacher MA, Funnell BE (2005) Structures of ParB bound to DNA reveal mechanism of partition complex formation. *Nature* 438(7067):516–519.
17. Schneidman-Duhovny D, Hammel M, Sali A (2010) FoXS: A web server for rapid computation and fitting of SAXS profiles. *Nucleic Acids Res* 38(Web Server issue): W540–W544.
18. Schneidman-Duhovny D, Hammel M, Tainer JA, Sali A (2013) Accurate SAXS profile computation and its assessment by contrast variation experiments. *Biophys J* 105(4): 962–974.
19. Kozin MB, Svergun DI (2001) Automated matching of high- and low-resolution structural models. *J Appl Cryst* 34(1):33–41.

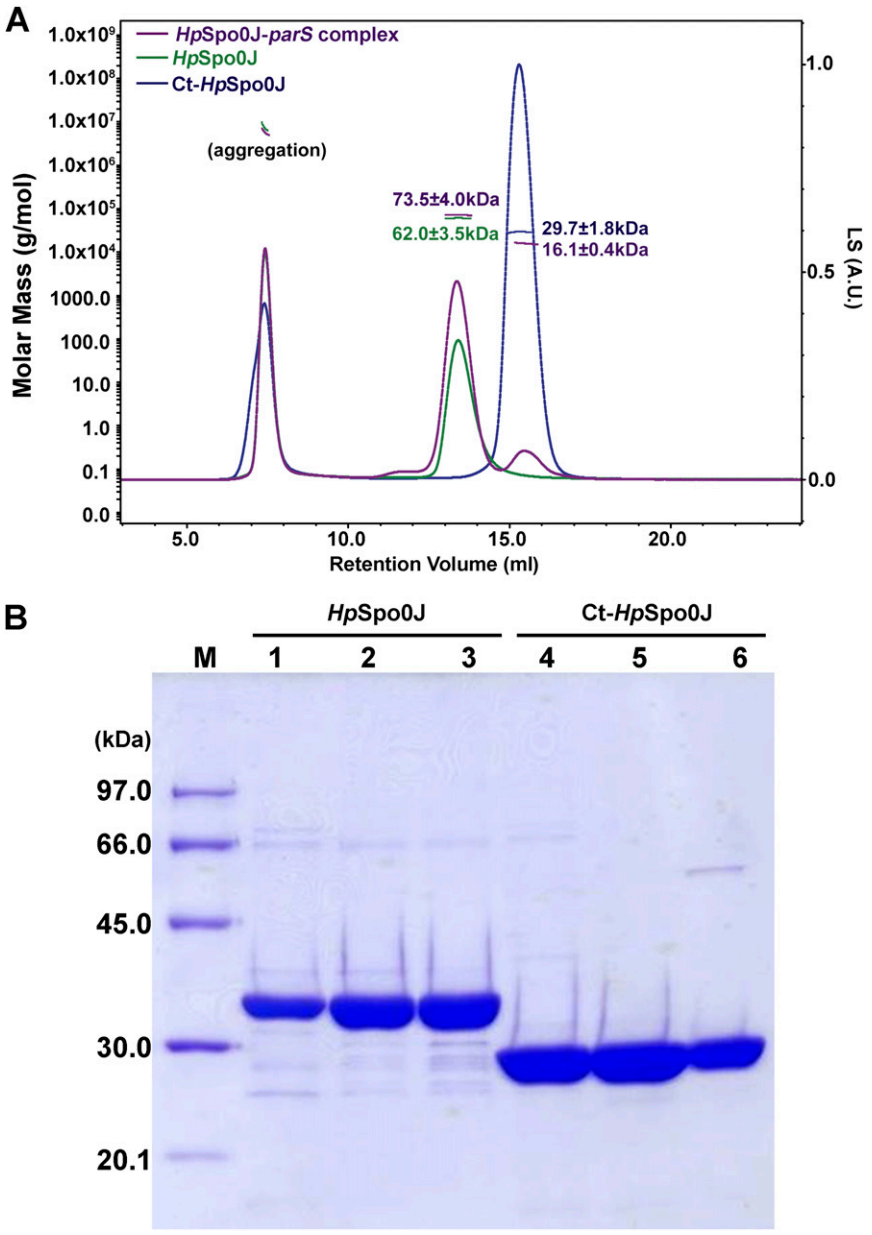

Fig. S1. Protein purification of *Hp*Spo0J, Ct-*Hp*Spo0J, and the *Hp*Spo0J–*parS* complex. (*A*) SEC-MALS results of full-length *Hp*Spo0J (green), Ct-*Hp*Spo0J (blue), and the *Hp*Spo0J–*parS* complex (purple) are shown. The aggregated protein samples were found before the void volume's peak (7.5 mL). Thin line segments represent the calculated molar masses, and the numbers denote the corresponding molecular weights of each peak (left *y* axis) in kilodaltons. The light scattering (LS) signal is also shown (right *y* axis). (*B*) SDS gels of *Hp*Spo0J (lanes 1–3) and Ct-*Hp*Spo0J (lanes 4–6), which were purified by Ni-NTA affinity column and eluted by buffer (20 mM Tris·HCl, pH 8.0, 420 mM NaCl, and 5 mM $MgCl_2$) with various imidazole concentrations (80, 110, and 220 mM). The protein markers (M: 20.1–97.0 kDa) are shown. The protein concentrations of *Hp*Spo0J (0.6 mg/mL; lane 2) and Ct-*Hp*Spo0J (0.9 mg/mL; lane 5) were determined by Beer's law, using absorbance assay of OD at 280 nm.

Fig. S2. Structural comparisons of monomers in the Ct-*Hp*Spo0J–*parS* complex. The structural superimposition of four monomers of Ct-*Hp*Spo0J: chains A (#55–226, green), B (# 35–226, purple), C (#45–227, orange), and D (#51–226, cyan) are shown. The RMSD of the overall structures of four Ct-*Hp*Spo0J monomers were calculated as 0.5–5.0 Å (Cα atoms). These four monomers share a similar DNA-binding domain but reveal various loops regions in the N-terminal domains, with an RMSD of 0.3–0.6 and 3.9–8.1 Å (Cα atoms) for DNA binding and N-terminal domains, respectively.

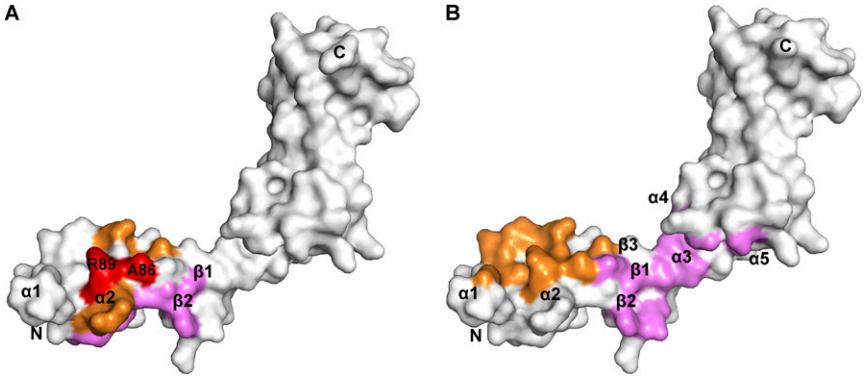

Fig. S3. The interfaces of AB and AC dimers of the Ct-*Hp*Spo0J–*parS* complex. (*A*) The interfaces of B and C molecules in AB and AC dimers. For the AB dimer, the interfaces of B molecule (magenta), β1, β2, loop β2-α2, and α2 used to interact with the A molecule are shown. For the AC dimer, the interfaces of C molecule (orange), loop α1-β1, β1, loop β2-α2, and α2 used to interact with the A molecule are shown. The overlap residues of interfaces of AB and AC dimers, Ala86 and Arg89 (red), are located at loop β2-α2 and α2, respectively. (*B*) The interfaces of A molecule in AB and AC dimers. For the AB dimer, the interaction interfaces of A molecule (magenta), β1, β2, loop β1–2, loop β3-α3, α3, loop α4–5, and α5, are used to approach the B molecule. For the AC dimer, the interaction interfaces of A molecule (orange), α1, loop α1-β1, β2, loop β2-α2, and α2, are used to approach the C molecule.

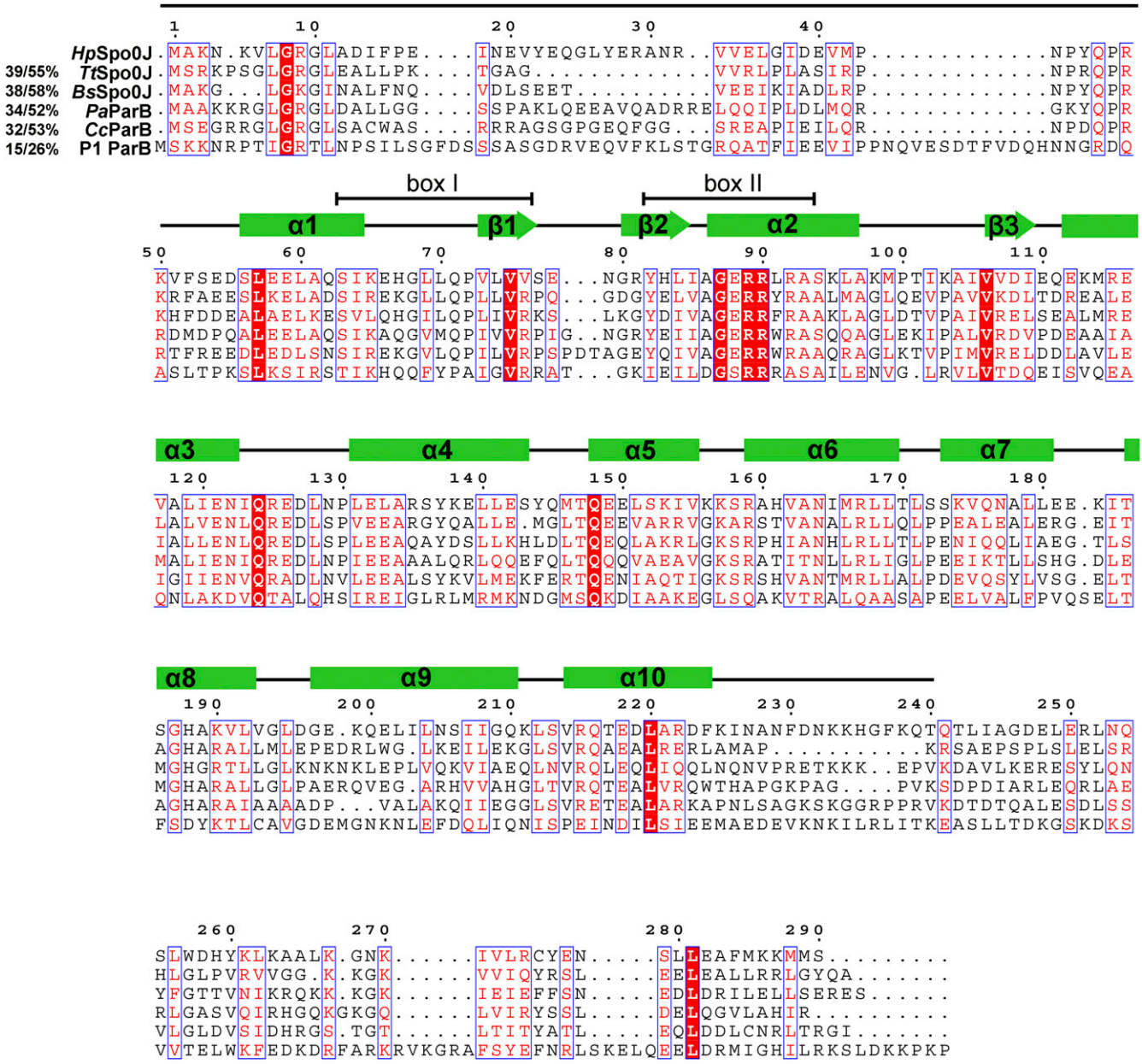

Fig. S4. Multiple sequence alignments of the ParB superfamily. Multiple sequence alignments of the ParB superfamily members from *Helicobacter pylori* (*Hp*Spo0J), *Thermus thermophilus* (*Tt*Spo0J), *Bacillus subtilis* (*Bs*Spo0J), *Pseudomonas aeruginosa* (*Pa*ParB), *Caulobacter crescentus* (*Cc*P1ParB), and *Enterobacteria phage* P1 (P1 ParB). Completely conserved residues are boxed in red, and conservatively exchanged residues are shown in red text. The residue numbering uses that of *Hp*Spo0J. Secondary-structure elements of *Hp*Spo0J are as cylinders and arrows for its α-helices (α1–10) and β-strands (β1–3), respectively. Box I (S63-V76) and box II (Y82-A93) are indicated.

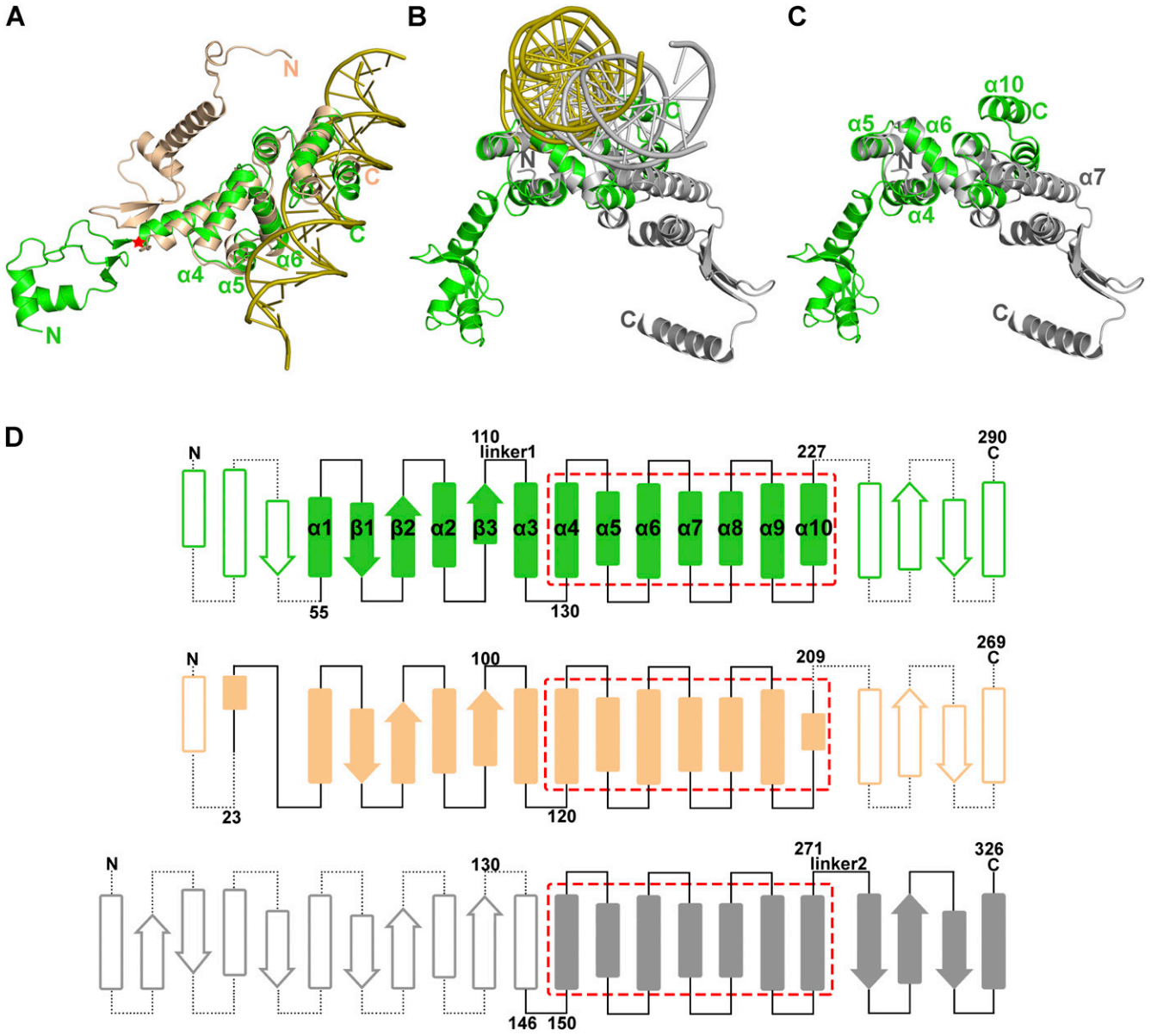

Fig. S5. Structural comparisons of *Hp*Spo0J vs. P1 ParB and *Tt*Spo0J. (*A*) The structural superposition of the Ct-*Hp*Spo0J–*parS* complex and DNA-free *Tt*Spo0J (wheat; PDB ID code 1VZ0) is shown. The RMSD of the HTH motif (α4–6) of *Tt*Spo0J and *Hp*Spo0J was calculated as 0.6 Å (Cα atoms). In the Ct-*Hp*Spo0J–*parS* complex, *parS* DNA is colored gold, and the linker sequence (residues E110–E112) is labeled with a red star. (*B* and *C*) The structural comparisons of *parS* binding domains of Ct-*Hp*Spo0J–*parS* and P1 ParB (gray; PDB ID code 1ZX4) complexes. In *C*, *parS* had been removed. The corresponding helices, α10 and α7, are labeled, respectively. (*D*) The secondary structure topologies of *Hp*Spo0J, *Tt*Spo0J (wheat), and P1 ParB (gray) are shown. The secondary structural elements determined by crystallography for *Hp*Spo0J are shown as solid rectangles and arrows for α-helices and β-strands, respectively. The predicted secondary structures are shown as hollow rectangles and arrows for α-helices and β-strands, respectively. The *parS* binding domains are boxed by red dashed lines. The *Hp*Spo0J and P1 ParB linker sequences are labeled 1 and 2, respectively. The residues numbers refer to the respective sequences.

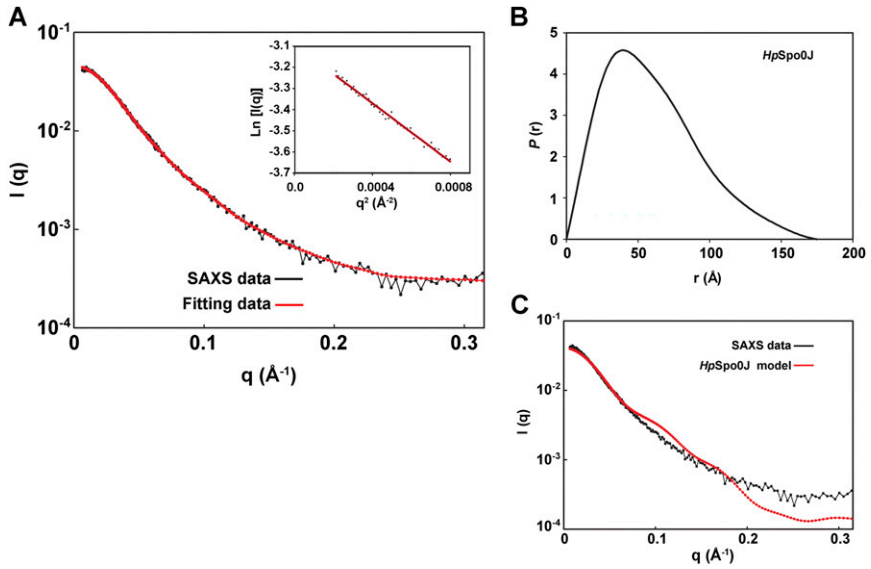

Fig. S6. SAXS characterization of *Hp*Spo0J. SAXS data were collected at beamline BL23A1 of the National Synchrotron Radiation Research Center (NSRRC) in Taiwan. (*A*) Experimental SAXS data (black line) and the theoretical fit of the data (red line) were generated by GNOM. (*Inset*) Guinier plots. (*B*) The distance distributions of *Hp*Spo0J. (*C*) Experimental SAXS data (black line) and the *Hp*Spo0J structural model of full-length *Hp*Spo0J (red line) fit by FoXS.

Table S1. Protein and DNA interactions in the Ct-*Hp*Spo0J–*parS* complex

Residue	*parS* DNA	Distance	Residue	*parS* DNA	Distance
		Hydrogen bond interactions			
Chain A			Chain B		
Gln148-N	T5 (OP2)	2.8 Å	Gln148-NE2	G6′ (OP2)	3.2 Å
Gln148-NE2	G6 (OP2)	2.7 Å	Lys157-NZ	G15 (OP1)	3.4 Å
Ser158-N	G16′ (OP2)	2.8 Å	Ser158-N	A16 (OP2)	2.5 Å
Ser158-OG	G16′ (OP2)	2.5 Å	Arg159-NH1	G6′ (O6)	2.7 Å
Arg159-NH2	G6 (OP2)	3.5 Å	Arg159-NH2	G6′ (O6)	2.7 Å
Asn164-ND2	T8 (O4)	3.5 Å	Asn164-ND2	T8′ (O4)	3.4 Å
Arg167-NE	T7 (OP2)	3.0 Å	Arg167-NE	T7′ (OP2)	2.7 Å
Gly187-N	T14′ (OP2)	3.1 Å	Gly187-N	T14 (OP2)	3.3 Å
Lys190-NZ	G15′ (O6)	2.9 Å	Lys190-NZ	T9′ (O4)	2.6 Å
Val214-N	G13′ (OP2)	3.0 Å	Val214-N	G13 (OP2)	2.5 Å
Arg215-NH2	T14′ (O4)	2.7 Å	Arg215-NH2	T14 (O4)	2.3 Å
Glu218-OE2	C10(N4)	3.4 Å	Glu218-OE2	C10′ (N4)	3.4 Å
			Arg222-NE	T9′ (OP2)	3.1 Å
			Arg225-NZ	T8′ (OP2)	3.4 Å
Chain C			Chain D		
Gln148-N	T5 (OP2)	3.1 Å	Gln148-N	T5 (OP2)	2.9 Å
Ser158-N	A16 (OP2)	2.8 Å	Lys157-NZ	G15′ (OP2)	2.5 Å
Arg159-NH2	G6′ (O6)	2.5 Å	Ser158-N	G16′ (OP2)	2.8 Å
His161-NE2	G15 (OP2)	3.4 Å	Arg159-NH2	G6 (O6)	2.3 Å
Asn164-ND2	T8′ (O4)	3.0 Å	Asn164-ND2	T8 (O4)	3.3 Å
Arg167-NH1	T7′ (OP2)	2.3 Å	Arg167-NH1	T7 (O5′)	2.7 Å
Gly187-N	T14 (OP2)	2.9 Å	Arg167-NH1	T7 (OP2)	3.1 Å
Lys190-NZ	G15 (O6)	3.3 Å	Gly187-N	T14′ (OP2)	3.4 Å
Val214-N	G13 (OP2)	2.7 Å	Val214-N	G13′ (OP2)	2.9 Å
Arg215-NH2	T14 (O4)	2.5 Å	Arg215-NH1	T14 (O4)	2.7 Å
Arg215-NH2	G13 (O6)	3.1 Å	Glu218-OE2	C10 (N4)	2.6 Å
Glu218-OE2	C10′ (N4)	3.5 Å	Arg222-NH2	C9 (OP2)	3.1 Å
Arg222-NH1	T9′ (OP2)	2.9 Å	Arg225-NZ	T8 (O5′)	3.3 Å
		Hydrophobic interactions			
Chain A			Chain B		
Gln148-CG	T5 (OP2)	3.4 Å	Thr147-CB	T5′ (OP2)	3.2 Å
Ala160-CB	A17′ (N6)	3.4 Å	Gln148-CG	T5′ (OP2)	3.0 Å
His161-CE1	G15′ (OP2)	3.2 Å	Ala160-CB	A17 (N6)	3.4 Å
Lys190-CE	C9 (N4)	3.0 Å	Lys190-CE	T9′ (O4)	3.1 Å
Ser213-CB	C12′ (OP2)	3.5 Å	Ser213-CA	G13 (OP2)	3.1 Å
Lys225-CE	T8 (OP1)	3.3 Å	Ser213-CB	G13 (OP2)	3.4 Å
Chain C			Chain D		
Gln148-CG	T5′ (OP2)	3.1 Å	Gln148-CB	T5 (OP2)	2.9 Å
Gln148-CB	T5′ (OP2)	3.3 Å	Ala160-CB	T7 (O4)	3.2 Å
Ser213-CA	G13 (OP2)	3.4 Å	Lys190-CE	C9 (N4)	3.0 Å
Lys225-CE	T8′ (OP1)	3.2 Å	Ser213-CA	G13′ (OP2)	3.4 Å
			Lys225-CE	T8 (OP1)	3.1 Å

Table S2. Dimer interfaces in the box I, box II (arginine patch) of the Ct-*Hp*Spo0J–*parS* complex

Chain A	Chain B	Distance	Chain C	Chain D	Distance
Adjacent interaction (crosswise dimer): Hydrogen bond interactions					
Met114-O	Arg89-NH2	3.3 Å	Gln47-NE2	Ser77-OG	2.7 Å
Arg115-NH2	Arg89-O	2.7 Å	Arg115-NH1	Val75-O	2.9 Å
Ser143-OG	Arg89-NH1	3.5 Å	Arg115-NH2	Val75-O	2.7 Å
Glu150-OE2	Arg49-NH2	3.1 Å	Gln145-O	Arg89-NH1	2.7 Å
			Gln145-O	Arg89-NH2	3.2 Å
Adjacent interaction (crosswise dimer): Hydrophobic interactions					
Val76-CG1	Ala86-CB	3.5 Å	Pro48-O	Glu110-CB	4.2 Å
Glu78-OE2	Val76-CG1	3.9 Å	Lys50-NZ	Glu110-CG	3.1 Å
His83-CD2	Leu84-CG	4.3 Å	Asn79-ND2	Lys98-CD	4.2 Å
Ile85-C	His83-NE2	3.7 Å	Leu84-CD1	Ser77-O	3.8 Å
Ile85-CA	Leu84-O	4.4 Å	Gln111-CB	Val76-CG2	3.8 Å
Gln-111-OE1	Ala86-CB	4.5 Å	Arg115-NE	Val76-CG2	3.3 Å
Arg115-NH1	Leu91-CA	3.9 Å	Arg115-CD	Lys95-CG	3.4 Å
Arg115-CD	Ser94-OG	4.2 Å	Asn122-OD1	Leu91-CD2	3.3 Å
Arg115-CD	Lys95-NZ	3.3 Å	Ile123-CD1	Arg92-NH2	3.2 Å
Val117-CG1	Arg89-NH2	3.8 Å	Gln145-O	Leu74-CD2	3.7 Å
Asn122-ND2	Arg91-CD1	3.3 Å	Met146-CA	Arg89-NH1	3.8 Å
Tyr144-CE1	Arg89-CB	3.3 Å	Glu150-OE2	Ile85-CG1	4.3 Å
			Glu150-OE2	Arg89-CD	3.1 Å
Transverse interaction (bridging dimer): Hydrogen bond interactions					
Gln62-OE1	—		Arg89-NH1	—	3.0 Å
Gln71-NE2	—		Val73-O	—	3.2 Å
Arg89-NH2	—		Arg89-O	—	2.6 Å
Transverse interaction (bridging dimer): Hydrophobic interactions					
Glu58-CG	—		Phe52-CD2	—	3.4 Å
Lys65-CD	—		Arg49-NH2	—	3.6 Å
His67-CE1	—		Glu88-OE2	—	3.2 Å
Leu70-CD2	—		Ala86-O	—	3.3 Å
Leu70-CD2	—		Gly87-CA	—	3.9 Å
Gln71-OE1	—		Leu74-CB	—	3.1 Å
Gln71-CB	—		Val75-CG1	—	3.5 Å
Gln71-O	—		Arg89-CD	—	3.6 Å
Leu74-CD1	—		Pro72-CB	—	3.6 Å
Ala86-CB	—		Gln71-NE2	—	3.5 Å
Arg89-NH2	—		Arg92-CD	—	3.5 Å
Arg90-CD	—		Arg89-NH2	—	3.0 Å

Table S3. X-ray diffraction data and refinement statistics of the Ct-*Hp*Spo0J–*parS* complex

	Ct-*Hp*Spo0J–*parS*	*Se*-Ct-*Hp*Spo0J–*parS*		
Parameters	Native	Peak	Inflection	Remote
Data collection				
Beamline	13C1	13B1	13B1	13B1
Wavelength (Å)	0.9750	0.9789	0.9790	0.9638
Space group	$P2_1$	$P2_1$	$P2_1$	$P2_1$
Cell dimensions				
a, *b*, *c* (Å)	54.5, 232.7, 78.3	54.5, 233.2, 78.2	54.5, 233.1, 78.2	54.4, 232.5, 78.0
α,β,γ (°)	90, 109.2, 90	90, 109.2, 90	90, 109.2, 90	90, 109.2, 90
Resolution (Å)*	30.0–3.1 (3.2–3.1)	30.0–3.2 (3.3–3.2)	30.0–3.2 (3.3–3.2)	30.00–3.2 (3.3–3.2)
R_{merge}*,†	6.9 (44.5)	9.9 (41.9)	8.9 (43.3)	8.4 (44.8)
$I/\sigma(I)$*	17 (3.1)	19 (6.3)	13 (3.1)	16 (3.1)
Completeness (%)*	99.8 (100)	97.6 (96.8)	96.5 (94.6)	95.5 (93.1)
Refl. total/unique	140,692/33,332	202,706/29,787	106,720/30,675	102,262/30,313
Redundancy*	4.2 (4.3)	6.8 (6.5)	3.5 (3.4)	3.4 (3.3)
Refinement				
Resolution (Å)	23.57–3.1			
No. reflections	32,160			
R_{work}	25.1			
R_{free}‡	29.9			
No. atoms	7,994			
Protein	5,765			
DNA	1,968			
Sulfate	30			
Water	231			
B-factors	67.7			
Protein	71.4			
DNA	57.9			
Sulfate	125.6			
Water	52.79			
Solvent content (%)	51			
RMSD				
Bond lengths (Å)	0.012			
Bond angles (°)	1.881			
PDB ID code	4UMK			

*Values in parentheses were for the highest-resolution shell.
†$R_{merge} = \Sigma_{hkl}\Sigma_i |I_i(hkl) - \langle I(hkl)\rangle| / \Sigma_{hkl}\Sigma_i I_i(hkl)$.
‡R_{free} factor calculated for 5% randomly chosen reflections not included in the refinement.